FEBS Open Bio 2 (2012) 298–304

FEBS openbio

journal homepage: www.elsevier.com/locate/febsopenbio

Experimental evidence for the involvement of amino acid residue Glu398 in the autocatalytic processing of *Bacillus licheniformis* γ-glutamyltranspeptidase

Meng-Chun Chi[a,1], Yi-Yu Chen[a,1], Huei-Fen Lo[b], Long-Liu Lin[a,*]

[a] Department of Applied Chemistry, National Chiayi University, Taiwan
[b] Department of Food Science and Technology, Hungkuang University, Taiwan

ARTICLE INFO

Article history:
Received 20 September 2012
Received in revised form 25 September 2012
Accepted 25 September 2012

Keywords:
Bacillus licheniformis
γ-Glutamyltranspeptidase
Glutamate
Site-directed mutagenesis
Autocatalytic processing

ABSTRACT

The role of glutamate 398 in the autocatalytic processing of *Bacillus licheniformis* γ-glutamyltranspeptidase (*Bl*GGT) was explored by site-directed mutagenesis. This glutamate was substituted by either alanine, aspartate, arginine or glutamine and the expressed mutant enzymes were purified to apparent homogeneity with metal-affinity chromatography. SDS–PAGE analysis showed that E398A, E398D and E398K were unable to process themselves into a large and a small subunit. However, E398Q was not only able to process itself, but also had a catalytic activity comparable to that of *Bl*GGT. As compared with the wild-type enzyme, no significant change in circular dichroism spectra was observed for the mutant proteins. Thermal unfolding of *Bl*GGT, E398A, E398D, E398K and E398Q followed the two-state unfolding process with a transition point (T_m) of 47.7–69.4 °C. Tryptophan fluorescence spectra of the mutant enzymes were different from the wild-type protein in terms of fluorescence intensity. Native *Bl*GGT started to unfold beyond ~1.92 M guanidine hydrochloride (GdnHCl) and reached an unfolded intermediate, $[GdnHCl]_{0.5,N-U}$, at 3.07 M equivalent to free energy change ($\Delta G^{H_2O}_{N-U}$) of 14.53 kcal/mol for the N → U process, whereas the denaturation midpoints for the mutant enzymes were 1.31–2.99 M equivalent to $\Delta G^{H_2O}_{N-U}$ of 3.29–12.05 kcal/mol. Taken together, these results strongly suggest that the explored glutamate residue is indeed important for the autocatalytic processing of *Bl*GGT.

1. Introduction

γ-Glutamyltranspeptidase (GGT) is a member of the N-terminal nucleophile (Ntn) hydrolase superfamily [1] and catalyzes the transfer of the γ-glutamyl moiety of glutathione to an acceptor that may be an amino acid, a short peptide or water [2]. The enzyme plays a key role in the γ-glutamyl cycle, a pathway for the synthesis and degradation of glutathione and drug and xenobiotic detoxification [3]. Mammalian GGT is a transmembrane glycoprotein with its active site exposed to the outside surface of the membrane, where γ-glutamyl moieties of glutathione are supposed to be cleaved and transferred to amino acids leading to the formation of γ-glutamyl amino acids that are then imported into the cell by glutathione-GGT-mediated amino acid transport pathway [4]. In this regard, the hydrolysis of the γ-glutamyl linkage of extracellular glutathione allows the cell to use this antioxidant compound as a good source of cysteine for the increased synthesis of intracellular glutathione [5]. As an antioxidant molecule, glutathione plays an important part in providing vital cellular protection against the reactive oxygen species, such as hydrogen peroxide, generated by aerobic respiration [6]. Thus, GGT-dependent breakdown of glutathione in eukaryotes aids maintenance of cellular glutathione levels and increased cellular resistance to hydrogen peroxide-induced injury [7]. In *Helicobacter pylori*, GGT has been shown to be involved in bacterial colonization of the gastric mucosa of mice [8,9], potentially by participating in the *de novo* synthesis of essential amino acids and thus enabling survival *in vivo*. The enzyme possesses an apoptosis-inducing activity [10] and can up-regulate COX-2 and EGF-related peptide expression in human gastric cells [11]. The contribution of GGT to *Campylobacter jejuni* virulence and colonization of the avian gut has also been reported [12]. Additionally, GGT appears to provide an advantage for the multiplication of *Neisseria meningitidis* during environmental cysteine shortage by supplying cysteine from environmental peptides [13].

GGT genes are translated as a unique polypeptide, which then undergoes an autocatalytic cleavage to form either a heterodimeric or heterotetrameric enzyme consisting of the typical large (L) and small (S) subunits. The molecular masses of the two chains are commonly found in a range of 38–72 kDa for the L subunit and 20–66 kDa for the S subunit [8,14–19], respectively. Such a high variation in the molecular masses of these two subunits can be adequately explained by the high

[1] These authors contributed equally to this work.

* Correspondence author. Address: Department of Applied Chemistry, National Chiayi University, 300 Syuefu Road, Chiayi County 60004, Taiwan. Tel.: +886 5 2717969; fax: +886 5 2717901.
E-mail address: llin@mail.ncyu.edu.tw (L.-L. Lin).

2211-5463/$36.00
http://dx.doi.org/10.1016/j.fob.2012.09.007

glycosylation of the animal and plant enzymes [20,21]. The amino acid sequence of the S subunits, which contains most of the residues required for the formation of catalytic site, is slightly more conserved than that of the L subunits [22,23]. Furthermore, a strictly conserved threonine residue in the S subunit of GGT enzymes, such as Thr391 of *Escherichia coli* GGT (*Ec*GGT) [24], Thr380 of *H. pylori* GGT (*Hp*GGT) [25] and Thr399 of *Bacillus licheniformis* GGT (*Bl*GGT) [26], serves as the N-terminal nucleophile and is essential for the maturation of the inactive precursors. The proposed mechanism for the autocatalytic processing of *Bl*GGT is shown in Fig. 1(A). Firstly, the hydroxyl group of the side chain of the conserved threonine residue of the precursor proteins performs a nucleophilic attack on the carbonyl group of the preceding glutamate residue to form a transitional tetrahedral intermediate. The cleavage of the C–N bond through protonation of the amino group of the Thr residue forms an ester intermediate (N–O acyl shift), which is then hydrolyzed by a water molecule to produce a L subunit and a S subunit.

The putative *B. licheniformis ggt* gene can be translated into a 61.259-kDa polypeptide precursor consisting of a signal peptide of 25 residues, a L-subunit of 374 residues, and a S-subunit of 187 residues (Swiss-Prot Q65KZ6). The *ggt* gene encoding *Bl*GGT was previously cloned and over-expressed in *E. coli* M15 cells [14]. Deletion analysis of the recombinant enzyme has demonstrated that the C-terminal sequences are critical for its functional expression in host cells [27]. Sequence comparison shows that a threonine residue (corresponds to Thr399 of *Bl*GGT) is strictly conserved in the aligned enzymes and mostly either a glutamine or a glutamate is present at the amino acid position corresponding to glutamate 398 of *Bl*GGT (Fig. 1(B)). Although the involvement of a conserved threonine residue in the autoproteolytic cleavage of GGT enzymes has been extensively explored [24–26,28], there is still no report dealing with the importance of the preceding glutamine/glutamate residue on the maturation process of the precursor proteins. In this study, we substituted glutamate 398 of *Bl*GGT with other amino acids in order to gain insight into the role of this residue. Mutations of this glutamate residue have been found to impair the autocatalytic processing of *Bl*GGT, indicating that it might play a crucial role in the maturation of enzyme precursor.

2. Results

2.1. Characterization of wild-type and mutant enzymes

Following expression and metal affinity chromatography, wild-type and mutant enzymes were subjected to SDS–PAGE analysis (Fig. 2). Gel electrophoresis results showed that the target proteins can be purified to near homogeneity from the crude extracts in a single chromatographic step. As shown in Fig. 2, most of *Bl*GGT and E398Q proteins were autocatalytically processed to yield a L subunit and a S subunit. The purified wild-type enzyme had a specific activity of 13.68 U/mg protein. The specific activity for E398K and E398Q was 0.25 and 12.71 U/mg protein, respectively, but the GGT activity was completely abolished in the remaining mutant enzymes.

The kinetic parameters for *Bl*GGT, E398K and E398Q were also determined. The K_M and k_{cat} values for *Bl*GGT were 0.39 mM and 23.3 s^{-1}, respectively. Kinetic values of E398Q were essentially consistent with those of the wild-type enzyme, whereas E398K showed more than 0.27-fold increase in K_M value and 57.3-fold decrease in k_{cat}, leading to 41.5-fold reduction in the catalytic efficiency. These results suggest that Glu398 is a crucial residue for *Bl*GGT.

2.2. Structural analyses

To evaluate how the secondary structural elements of *Bl*GGT were affected by the mutations, we analyzed far-UV CD spectral profiles of wild-type and mutant enzymes. The CD spectrum of *Bl*GGT displayed strong peaks of negative ellipticity at 208 and 222 nm, indicative of a

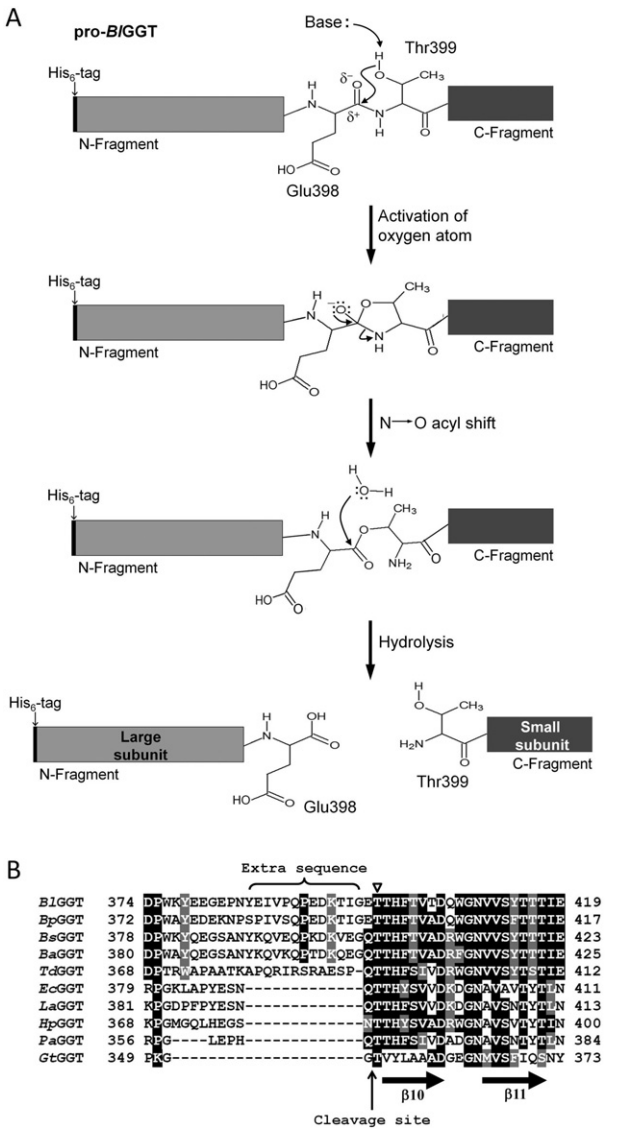

Fig. 1. The proposed mechanism for the autocatalytic processing (A) and sequence alignment of GGT enzymes surrounding Glu398 and Thr399 of *Bl*GGT (B). The deduced amino acid sequences for *Bl*GGT (Swiss-Prot Q62WE3), *Bacillus pumilus* GGT (*Bp*GGT; Swiss-Prot F8SVM6), *Bacillus subtilis* GGT (*Bs*GGT; Swiss-Prot P54422), *Bacillus amyloliquefaciens* GGT (*Ba*GGT; Swiss-Prot F4ELE6), *Thiobacillus denitrificans* GGT (*Td*GGT; Swiss-Prot Q3SJ07), *Ec*GGT (Swiss-Prot P18956), *Labrenzia aggregate* GGT (*La*GGT; Swiss-Prot A0NWX8), *Hp*GGT (Swiss-Prot O25743), *Pseudomonas aeruginosa* GGT (*Pa*GGT; Swiss-Prot Q91406), and *Gt*GGT [28] are shown. Gaps in the aligned sequences (dashes) were introduced to maximize similarity. The vertical arrow shows the putative cleavage site and the nucleophilic threonine residue is indicated by an open triangle.

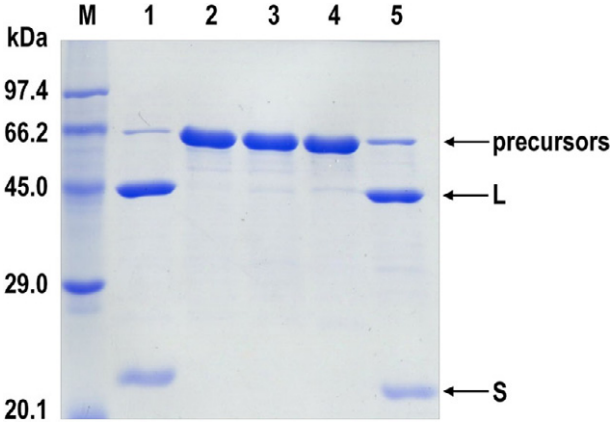

Fig. 2. Analysis of *Bl*GGT and its variants by SDS–PAGE. Lanes: M, protein size marker; 1, *Bl*GGT; 2, E398A; 3, E398D; 4, E398K; and 5, E398Q.

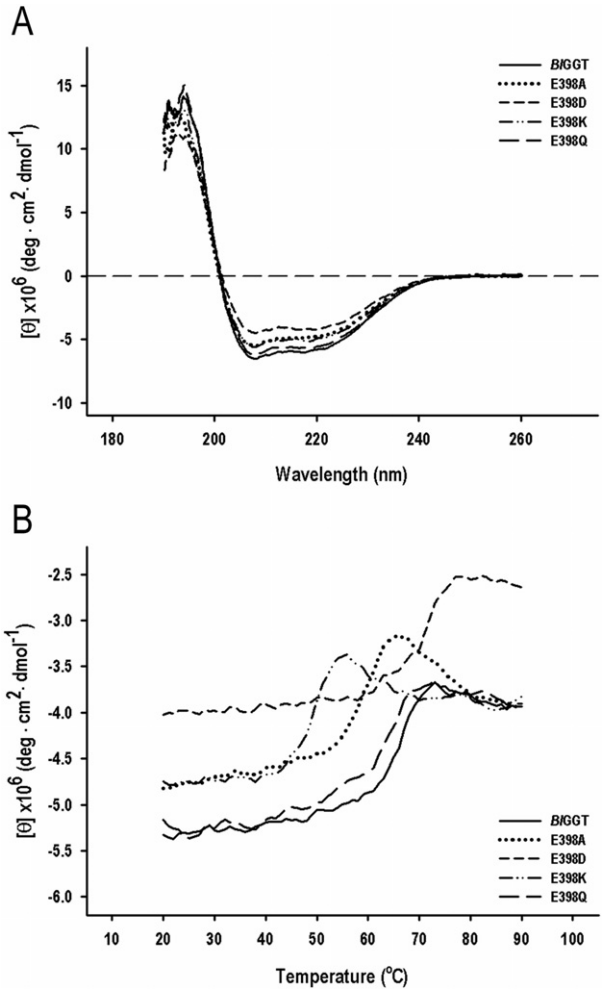

Fig. 3. CD analyses of wild-type and mutant *Bl*GGTs. (A) Far-UV spectra of *Bl*GGT and its variants. The data were recorded at 22 °C and residual molar elliticities of the protein samples in 50 mM Tris–HCl buffer (pH 9.0) were measured from 190 to 250 nm. (B) Temperature-induced denaturation of *Bl*GGT and its variants. The protein samples in 50 mM Tris–HCl buffer (pH 9.0) were monitored with the CD signal at 222 nm.

substantial α-helical content (Fig. 3(A)). The spectrometric characteristic of all mutant enzymes strongly resembled those of the wild-type protein. The spectra were further quantitatively analyzed by the DICHOWER server [29]. The normalized root-mean-square derivation values of the data fitting for *Bl*GGT and its variants were found to be less than 0.1 units, reflecting an excellent quality of the fit parameters [30]. The helical contents of *Bl*GGT, E398A, E398D, E398K, and E398Q were calculated to be 44%, 44%, 41%, 41%, and 42%, respectively, and the β-sheet contents were 17%, 20%, 21%, 20%, and 19%, respectively. These values confirm that no notable change in the secondary structural elements of *Bl*GGT has been occurred as a consequence of mutations.

Thermal unfolding transitions of wild-type and mutant *Bl*GGTs followed by the loss of ellipticity at 222 nm with the increase of temperature was also investigated (Fig. 3(B)). The transition for *Bl*GGT started at about 48 °C and had a midpoint of 64 °C. The T_m value of E398Q was close to the wild-type enzyme, whereas the midpoint temperatures for the inactive variants were dramatically decreased to less than 56 °C. These results clearly indicate that replacement of glutamate 398 with alanine, aspartate, or arginine has a detrimental effect on the thermal stability of *Bl*GGT.

Fluorescence spectra provide a sensitive means to analyze proteins and their confirmation. The spectrum is determined chiefly by the polarity of the environment of the tryptophan residue and by any specific interactions with nearby side chains [31]. Based on this principle, tryptophan fluorescence spectrum of *Bl*GGT was characterized by a peak centered at 343 nm (Fig. 1S). The mutant enzymes had fluorescence spectra qualitatively similar to that of the wild-type protein. However, the fluorescence intensity of mutant proteins was either quenched by 4.2–7.4% or enhanced by 6.7–51% with respect to *Bl*GGT. These observations suggest that amino acid replacements at position 398 cause minor structural changes in the enzyme.

2.3. Unfolding of BlGGT and its variants by GdnHCl

The functionality of proteins depends on their ability to acquire a unique tertiary structure. GdnHCl is commonly used as a protein denaturant to generally bring about unfolding of proteins by disrupting their secondary and tertiary structures [32]. Since *Bl*GGT has a total of four tryptophanyl residues, GdnHCl-induced unfolding is very suitable for studying the conformational stability of the enzyme and its variants. Unfolding of these proteins at different concentrations of GdnHCl was therefore performed and the experimental data were shown in Fig. 4(A). The AEW, which is simply the intensity weighted average of all of the wavelengths scanned, was used to calculate the thermodynamic parameters of the unfolding process. The wild-type enzyme started to unfold at 1.92 M denaturant with $[GdnHCl]_{0.5,N-U}$ of 3.07 M. The calculated free energy change ($\Delta G^{H_2O}_{N-U}$) for the N → U process is 14.53 kcal/mol. The fluorescence signal of mutant enzymes also followed a monphasic process (Fig. 4(A)), which showed $[GdnHCl]_{0.5,N-U}$ of 1.31–2.99 M corresponding to of 3.29–12.05 kcal/mol for the N → U process.

GdnHCl-induced unfolding of *Bl*GGT and its variants was also carried out to explore the effect of this denaturant on their secondary structure. The effect of increasing GdnHCl concentrations on the ellipticity of *Bl*GGT at 222 nm is illustrated in Fig. 4(B). A large decrease in the negative ellipticity was observed at GdnHCl concentrations between 2.4 and 3.1 M, indicating a significant disruption in the secondary structure of the enzyme under these conditions. It is worth noting that E398K was very sensitive to GdnHCl-induced denaturation respective to the wild-type enzyme. By fitting with Eq. (2), *Bl*GGT showed $[GdnHCl]_{0.5,N-U}$ of 2.86 M, corresponding to a free energy change of 13.04 kcal/mol for the N → U process. The $[GdnHCl]_{0.5,N-U}$ value of four mutant enzymes was in the range of 1.35–2.97 M equivalent to a free energy change of 5.45–12.29 kcal/mol.

2.4. In vitro maturation of the purified proteins

Maturation of the purified proteins in the elution buffer was monitored at 4 °C. At the indicated time intervals, the amount of precursors was recorded and the GGT activity was simultaneously assayed. As shown in Figs. 5(A) and 2S, *Bl*GGT and E398Q were mainly present as a mature form after the affinity chromatography. Almost all the precursors of these two proteins were processed within the first week of incubation. The autocatalytic processing of E398A and E398K occurred very slowly compared to the wild-type protein (Fig. 5(A)). However, E398D was not processed at all even after two months of incubation. The GGT activity of E398A and E398K increased linearly during the first month of maturation and was entering a retarded stage beyond the incubation period of 35 days (Fig. 5(B)). As expected, the unprocessed variant E398D was inactive all the time. These observations indicate that amino acid side chains at position 398 play a fundamental role in the maturation of *Bl*GGT.

3. Discussion

A general feature for the members of the Ntn-hydrolase superfamily is the autocatalytic processing of inactive precursors to generate a catalytic serine, threonine, or cysteine at their N-terminal ends [1,33].

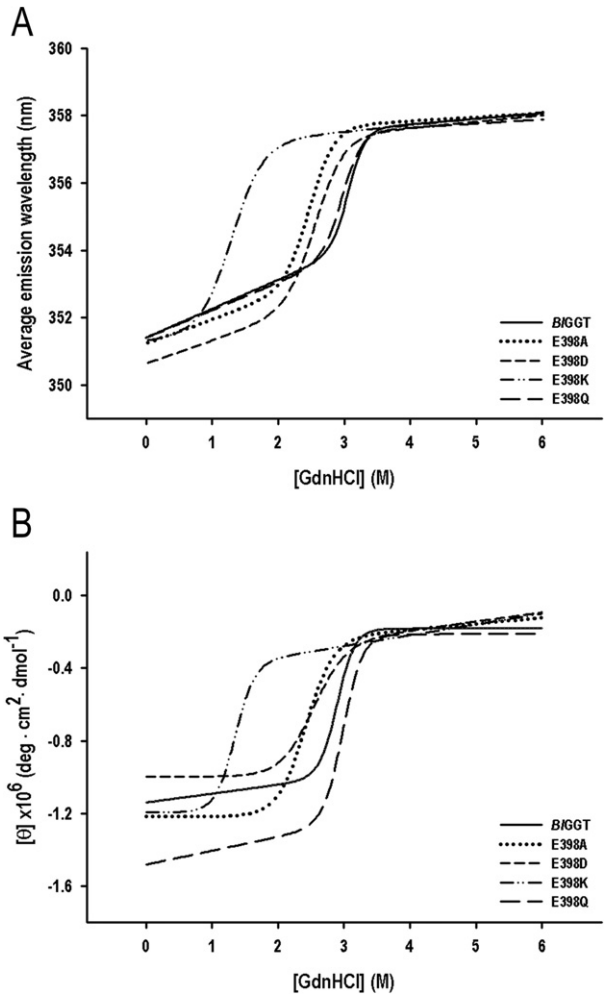

Fig. 4. GdnHCl-induced denaturation of *Bl*GGT and its variants. (A) Changes in intrinsic tryptophan fluorescence of the tested proteins as a function of GdnHCl concentration. Data are represented as the AEW, taking the value observed for native protein in absence of GndHCl as the control. (B) GdnHCl-induced changes in the secondary structures of *Bl*GGT and its variants as monitored by the negative ellipticity of the protein sample at 222 nm.

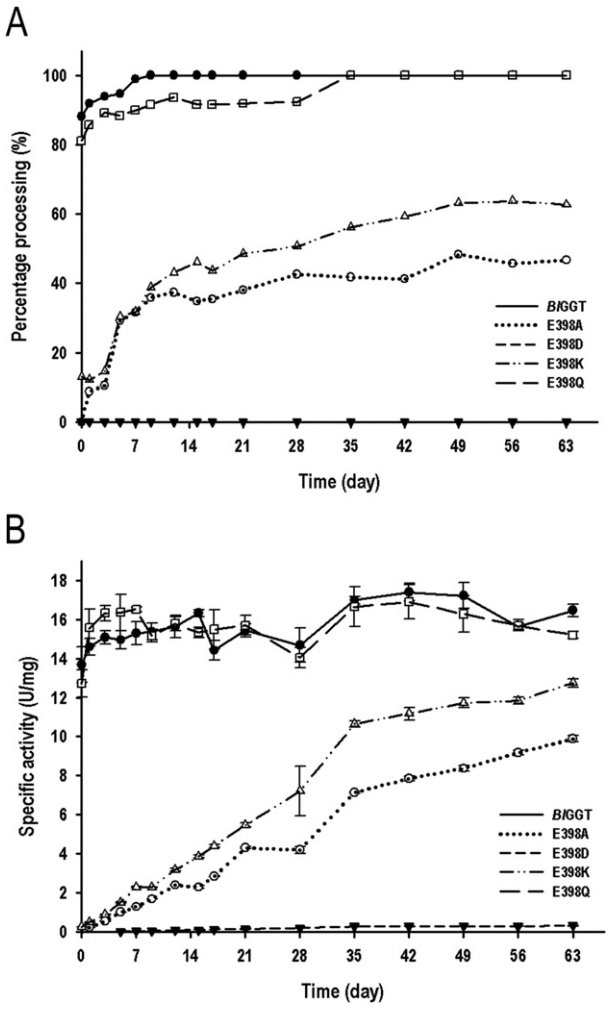

Fig. 5. Autocatalytic processing of *Bl*GGT and its variants. The protein samples were incubated for a period of time and aliquots were withdrawn at the indicated intervals for processing analysis (A) and GGT activity assay (B).

Site-directed mutagenesis of the catalytic threonine residue of GGT enzymes definitely creates a protein unable to carry out the autocatalytic maturation. In the cases of *Hp*GGT and *Ec*GGT, substitution of this threonine residue by Ala has been shown to result in the formation of an inactive and homodimeric precursor [34,35]. However, the corresponding replacement in *Gt*GGT leads to the production of a homotetrameric precursor with a low hydrolase activity, which has been proposed due to a solvent molecule that mimics the hydroxyl group of the catalytic threonine side chain [28]. Although all these studies have proved the involvement of a conserved Thr residue in the autocatalytic processing of GGT enzymes, role exploration into amino acid residues situated at the vicinity of this catalytic Thr residue is mostly lacking. As shown in Fig. 1(B), either a glutamate or a glutamine corresponding to amino acid position 398 of *Bl*GGT is largely present in the preceding position of the catalytic Thr residue. The conservation of these two kinds of residues throughout the evolution of GGT enzymes allowed us to make rational prediction of their structural importance. In fact, except for the glutamine replacement, our mutagenesis results have shown that glutamate 398 could not be replaced without affecting the maturation of this enzyme.

The structure of the inactive precursor is known for a number of Ntn-hydrolases, including aspartylglucosaminidase [36], proteasome [37], glutaryl 7-aminocephalosporanic acid acylase [38], and GGT [35]. The structural information has been collected by exploring the mutagenized native polypeptides with a prevented or delayed activation step. Several other publications of Ntn-hydrolases have further provided insights into the molecular details of precursor processing [24,39–43]. In an autocatalytic reaction, the hydroxyl oxygen of the side chain of the catalytic Thr residue forms a covalent bond to the carbonyl carbon of the preceding residue probably resulting in a tetrahedral intermediate, which may be stabilized by an oxyanion hole [36,42]. In bacterial AGA precursor structures, they contain a high-energy distorted *trans* peptide bond between Thr206 and its preceding residue [36], which is a potential driving force for the N → O shift [44]. Accordingly, conformational strain of the activation site was reported in proteasome [37] and glutaryl 7-aminocephalosporanic acid acylase [38]. Oligomerization of AGA precursor molecules has been further elucidated as a prerequisite for the autocatalytic activation [42,44] and may create a conformational strain at the activation site, which is released by the cleavage of the scissile peptide bond. In this research, the biophysical data reveal that E398Q protein is structurally similar to the wild-type enzyme. However, the remaining variants have a different conformation with respect to *Bl*GGT, and thus it would be speculative to conclude that the presence of Ala, Lys and Asp at amino acid position 398 can be detrimental to the autocatalytic processing of the enzyme. The *in vitro* maturation of E398A, E398K and E398D further proved that these replacements have a negative effect on the autocatalytic processing of *Bl*GGT (Fig. 5). Although the

structural information of GGT precursor proteins is still limited, *E. coli* T391A protein may provide a structural basis for a better understanding of the autocatalytic processing mechanism of this enzyme group [35]. We therefore modeled the molecular structure of *Bl*GGT precursor protein using *E. coli* T391A protein as the template. As shown in Fig. 6(A), the local confirmations of Ala399 of the T399A protein and Thr399 of the mature *Bl*GGT are very similar. Interestingly, a water molecule has been proposed to enhance the nucleophilicity of the Oγ atom of Thr391 [24]. The distances between the corresponding water and Ile396 O and Gly482 N of T399A protein are 2.6 and 2.8 Å, respectively. When the model of mature *Bl*GGT is superimposed with that of T399A protein, the distance between this water and Thr399 Oγ is estimated to be 2.7 Å. It is likely that rotation around the Cα–Cβ bond of Thr399 and displacement of this water molecule occur in the precursor protein so as to optimize the hydrogen-bonding geometry with its surrounding residues (Fig. 6(A)). Moreover, the Oγ atom of Thr399 is located at the carbonyl carbon atom between Glu398 and Thr399. This geometry facilitates the nucleophilic enhancement of Thr399 Oγ by the water. With the attack of Thr399 Oγ on the Glu398 C, the carbonyl carbon might adopt a tetrahedral arrangement and the collapse of the tetrahedral arrangement of Glu398 C shifts the linkage from an amide bond between Glu398 and Thr399 to an ester bond between the carbonyl group of Glu398 and the side-chain oxygen atom of Thr399 (N–O acyl shift). The intermediate ester bond formed by N–O acyl shift is subsequently hydrolyzed to generate the L- and S-subunits. It is worth noting that Glu398 O is hydrogen-bonded to the N atom of Leu421, which may help stabilize the orientation of Glu398 O. The conservation of this hydrogen bond in T398Q could be the major reason for the proper processing of the enzyme precursor. In contrast, the hydrogen-bonded interaction is abolished upon the replacement of Thr399 by Ala, Asp, and Lys (Fig. 6(B)–(D)). The loss of this interaction in T399A, T399D and T399K would alter the microenvironment around amino acid position 398 and such changes could be responsible for the delayed or prevented autocatalysis.

In conclusion, a glutamate residue Glu398 required for the autocatalytic processing of *Bl*GGT was identified by bioinformatics approaches. Amino acid residues located at the corresponding position have been proposed to be critical for the creation of the conformational strain at the cleavage site of some members of Ntn-hydrolases [37,38]. Our current investigations implicate that Glu398 might play a consistent role in the generation of the proper conformation at the cleavage site of *Bl*GGT. The experimental results also provide a solid foundation for further studies on other amino acid residues that participate in the maturation of GGT precursors.

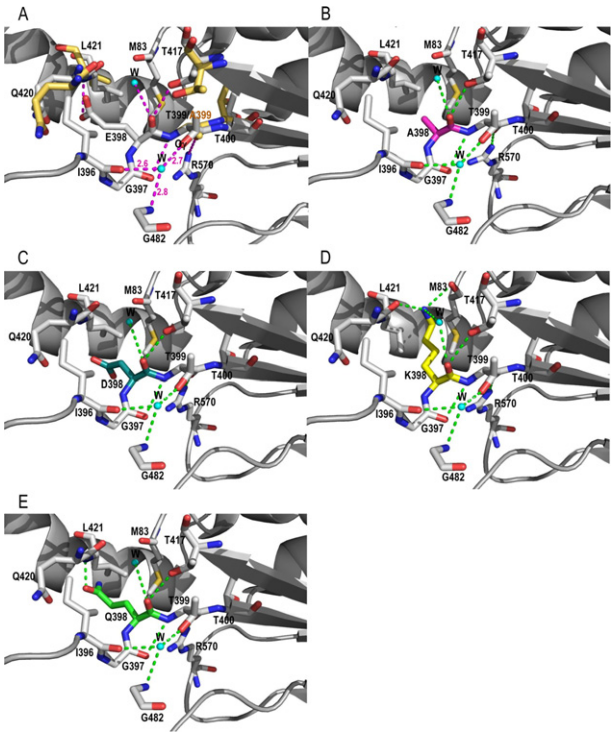

Fig. 6. The local structures around the autocatalytic site site of *Bl*GGT and its variants. These structures were constructed on the basis of the crystal coordinate structure of *Ec*GGT T391A protein. After the computer modeling, the respective structures were plotted by the program PyMOL. Panels: (A) superimposition of *Bl*GGT and T399A protein; (B) E398A; (C) E398D; (D) E398K; and (E) E398Q.

Table 1
Overlapping complementary primers used in the site-directed mutagenesis.

Protein	Nucleotide sequence (5′ → 3′)[a]	Codon change
E398A	(f)-AAAACGATCGGGGCGACGACGCATTTT	GAG → GCG
	(r)-AAAATGCGTCGTCGCCCCGATCGTTTT	
E398D	(f)-AAAACGATCGGGGACACGACGCATTTT	GAG → GAC
	(r)-AAAATGCGTCGTGTCCCCGATCGTTTT	
E398K	(f)-AAAACGATCGGGAAAACGACGCATTTT	GAG → AAA
	(r)-AAAATGCGTCGTTTTCCCGATCGTTTT	
E398Q	(f)-AAAACGATCGGGCAGACGACGCATTTT	GAG → CAG
	(r)-AAAATGCGTCGTCTGCCCGATCGTTTT	

[a] The altered codons were underlined.

4. Experimental procedures

4.1. Materials and growth conditions for Escherichia coli strains

Mutagenic primers were synthesized by Mission Biotechnology Inc. (Taipei, Taiwan). A QuikChange II site-directed mutagenesis kit was obtained from Stratagene (La Jolla, CA, USA). Nickel nitrilotriacetate (Ni^{2+}-NTA) was purchased from Qiagen Inc. (Valencia, CA, USA). Determination of transpeptidase activity was performed with L-γ-glutamyl-*p*-nitroanilide (L-γ-Glu-*p*-NA), Gly–Gly and *p*-nitroaniline (*p*-NA), which were acquired from Sigma–Aldrich Chemicals (St. Louis, MO, USA). Protein assay reagents, acrylamide, bis-acrylamide, TEMED, and ammonium persulfate were brought from Bio-Rad Laboratories (Hercules, CA, USA). Unless indicated otherwise, all other chemicals were of the highest purity available.

Escherichia coli strains were grown aerobically in Luria-Bertani (LB) medium at (1% bactotryptone, 0.5% yeast extract, and 1% NaCl; pH 7.0) at 37 °C. As required, antibiotics ampicillin and kanamycin were supplemented to LB medium at a final concentration of 100 and 25 μg/ml, respectively.

4.2. Site-directed mutagenesis and protein analyses

Plasmid pQE-*Bl*GGT [14] was used as a template for site-directed mutagenesis. Two overlapping complementary primers containing the desired nucleotide changes were designed for each mutation (Table 1). Four variants (E398A, E398D, E398K and E398Q) were constructed by a QuikChange II site-directed mutagenesis kit according to the manufacturer's protocol. Mutations were confirmed by DNA sequencing, which was carried out with dye terminator cycle sequencing and an automatic DNA sequencer. The verified plasmids were designed pQE-*Bl*GGT/D398A, pQE-*Bl*GGT/D398D, pQE-*Bl*GGT/D398K and pQE-*Bl*GGT/D398Q, respectively.

Wild-type and mutant enzymes were over-expressed in recombinant *E. coli* M15 cells and purified as described previously [45,46]. Protein purity and autocatalytic processing were checked by SDS–PAGE with the Laemmli buffer system [47]. Protein concentrations

were determined using the Bio-Rad protein assay reagent and bovine serum albumin as a standard protein.

4.3. Activity assay and determination of kinetic parameters

The standard GGT activity was assayed at 40 °C with L-γ-Glu-*p*-NA as the γ-glutamyl donor substrate and the dipeptide Gly–Gly as the acceptor substrate [14]. The reaction mixture contained 1.25 mM L-γ-Glu-*p*-NA, 30 mM Gly–Gly, 1 mM $MgCl_2$, 50 mM Tris–HCl buffer (pH 9.0), 20-μl enzyme solution at a suitable dilution, and enough distilled water to bring the final volume to 1 ml. After the incubation period of 10 min, the enzymatic reaction was quenched by the addition of 100 μl acetic acid (3.5 N) into the solution. The formation of *p*-NA was recorded by monitoring the absorbance changes at 410 nm. One unit of GGT activity is defined as the amount of enzymes that release 1 μmol of *p*-NA per minute under the standard assay conditions.

The K_M and k_{cat} values were estimated by measuring *p*-NA production in 1 ml reaction mixtures with various concentrations of L-γ-Glu-*p*-NA (0.1–2.0 K_M) and a fixed concentration (30 mM) of Gly–Gly in 50 mM Tris–HCl buffer (pH 8.0). To estimate the kinetic constants, a Lineweaver–Burk plot was fitted using GRAF4WN softwares. All the reactions were performed at least three times.

4.4. Circular dichroism (CD)

All far-UV CD studies were performed on a JASCO-815 spectrometer equipped with a temperature-controlling liquid nitrogen system. Protein samples were adjusted with 50 mM Tris–HCl buffer (pH 9.0) to a concentration of approximately 12.4 μM before the spectral analyses. Far-UV CD spectra were taken over the wavelength range from 190 to 250 nm with a 2-mm path length cell. The photomultiplier absorbance was always controlled below 600 V in the analyzed region. Ten spectra were averaged for each protein sample and the obtained data were carefully corrected by subtracting buffer contribution from parallel spectra in the absence of protein. The data were expressed as molar ellipticity (deg cm^2 $dmol^{-1}$) based on a residue number of 612 and a mean molecular weight (MRW) of 65.9 kDa. Molar ellipticity was calculated as $[\theta] = [100 \times (\mathrm{MRW}) \times \theta_{obs}/(c \times l)]$, where θ_{obs} represents the observed ellipticity in degree at a given wavelength, c is the protein concentration in mg/ml, and l is the length of the light path in cm.

Temperature-induced unfolding of wild-type and mutant proteins (12.4 μM each) in 50 mM Tris–HCl buffer (pH 9.0) was followed by monitoring the change in ellipticity at 222 nm. Protein samples were heated with a scan rate of 2 °C/min. The changes in ellipticity (θ) at 222 nm were analyzed according to Eq. (1) [48].

$$\theta_{222} = \frac{\theta_N + \theta_U \cdot \exp\left[-\frac{\Delta H_U}{RT}\cdot\left(1-\frac{T}{T_m}\right)+\frac{\Delta C_{PU}}{RT}\cdot\left(T\ln\left(\frac{T}{T_m}\right)+T_m-T\right)\right]}{1+\exp\left[-\frac{\Delta H_U}{RT}\cdot\left(1-\frac{T}{T_m}\right)+\frac{\Delta C_{PU}}{RT}\cdot\left(T\ln\left(\frac{T}{T_m}\right)+T_m-T\right)\right]} \quad (1)$$

where θ_{222} is the relative ellipticity at 222 nm, θ_N and θ_U are the calculated ellipticities of the native and unfolded states, respectively, ΔH_U is the free enthalpy of unfolding, ΔC_{PU} is the heat capacity of unfolding, T_m is the transition midpoint temperature, T is temperature, and R represents the universal gas constant.

4.5. Fluorescence spectroscopy

Fluorescence spectra of *Bl*GGT and its variants were monitored at 25 °C in a JASCO FP-6500 fluorescence spectrophotometer with an excitation wavelength of 280 nm. All spectra were corrected for the contribution of 50 mM Tris–HCl buffer (pH 9.0). The fluorescence emission spectra of protein samples with a concentration of 12.4 μM were recorded from 300 to 400 nm at a scanning speed of 240 nm/min. The maximal peak of fluorescence spectrum and the change in fluorescence intensity were used in monitoring the unfolding processes of parental and mutant proteins. Both the shift of wavelength and the change of fluorescence intensity were analyzed together using the average emission wavelength (AEW) [49].

4.6. Guanidine hydrochloride (GdnHCl)-induced unfolding

Wild-type and mutant *Bl*GGTs were unfolded with different concentrations of GdnHCl in 50 mM Tris–HCl buffer (pH 9.0) at room temperature. An incubation period of 30 min was initially found to be sufficient for the unfolding process. Unfolding curves of CD and fluorescence spectroscopy were subsequently used to calculate the thermodynamic parameters by global fitting of the experimental data. The two-state unfolding model was described by Eq. (2) [50].

$$y_{obs} = \frac{(y_N + m_f[D]) + (y_U + m_u[D])\cdot\exp\left[-(\Delta G^{H_2O}_{N-U} - m[D])/RT\right]}{1+\exp\left[-(\Delta G^{H_2O}_{N-U} - m[D])/RT\right]} \quad (2)$$

Then, $[\mathrm{GdnHCl}]_{0.5,N-U}$ could be calculated by the equation below:

$$[\mathrm{GdnHCl}]_{0.5,N-U} = \frac{\Delta G^{H_2O}_{N-U}}{m} \quad (3)$$

where y_{obs} is the observed biophysical signal (molar ellipticity for CD and AEW for fluorescence spectroscopy), y_N and y_U are the intercepts, m_f and m_u are the slopes of the pre- and post-transition baselines, T is temperature, R is the universal gas constant, $[D]$ is the concentration of GdnHCl, $\Delta G^{H_2O}_{N-U}$ represents free energy change for the N → U process, and m is a measure of the dependence of ΔG on GdnHCl concentration.

4.7. Precursor autoprocessing

The purified samples (500 μl) at a protein concentration of approximately 0.94 mg/ml were incubated at 4 °C and 16 μl was removed at fixed time-intervals. The autoprocessing reaction was stopped by boiling the sample for 3 min and the samples were subsequently subjected to SDS–PAGE analysis. The electrophoresed gels were stained with Coomassie Brilliant Blue R-250 and the exposure time for the gel stains was set at 10 min to unify the conditions and to reduce the possibility of overexposure. The amounts of the unprocessed *Bl*GGT precursor were quantified by densitometry using CP ATCAS 2.0 program (http://www.lazarsoftware.com). The scanned intensity of the *Bl*GGT precursor band was plotted against time and processing percentages were calculated from the single-exponential fit.

4.8. Computer modeling

Construction of molecular models, structure optimization, and conformational analyses were carried out with the Discovery Studio 1.7 (Accelrys Inc., Burlington, MA, USA) using the CHARMM empirical force field [51]. The molecular structure of *Bl*GGT precursor protein was firstly constructed at SWISS MODEL Server [52] with the X-ray crystal structure of *Ec*GGT (PDB code: 2EDW). The modeled structures were further energy minimized at iterated 500 cycles using the Steepest Descent methods and finally convergence at 0.002 kcal/mol Å.

Acknowledgements

The authors are very grateful to Dr. Ching-Yuh Chen for the valuable discussions on experimental results. The present work was supported by grants from National Science Council of Taiwan (NSC 97–2628-B-415–001-MY3 and NSC 100–2313-B-415–003-MY3).

Supplementary Material

Supplementary material associated with this article can be found, in the online version, at doi:10.1016/j.fob.2012.09.007.

References

[1] Brannigan JA, Dodson G, Duggleby HJ, Moody PC, Smith JL, Tomchick DR et al. (1995) A protein catalytic framework with an N-terminal nucleophile is capable of self-activation. Nature. 90, 416–419.

[2] Tate SS, Meister A (1985) γ-Glutamyltranspeptidase from kidney. Meth. Enzymol. 113, 400–419.

[3] Siest G, Courtay C, Oster T, Michelet F, Visvikis A, Diederich M et al. (1992) γ-Glutamyltransferase: nucleotide sequence of the human pancreatic cDNA: evidence for a ubiquitous γ-glutamyltransferase polypeptide in human tissues. Biochem. Pharmacol. 43, 2527–2533.

[4] Meister A, Anderson ME (1983) Glutathione. Annu. Rev. Biochem. 52, 711–760.

[5] Stipanuk MH, Dominy Jr JE, Lee JI, Coloso RM (2006) Mammalian cysteine metabolism: new insights into cysteine metabolism. J. Nutr. 136, 16525–16595.

[6] O'Donovan DJ, Fernandes CJ (2000) Mitochondrial glutathione and oxidative stress: implications for pulmonary oxygen toxicity in premature infants. Mol. Genet. Metab. 71, 352–358.

[7] Shi M, Gozal E, Choy HA, Forman HJ (1993) Extracellular glutathione andγ-glutamyltransferase prevent H_2O_2-induced injury by 2,3-dimethyl-1,4-naphthoquinone. Free Radical Biol. Med. 15, 57–67.

[8] Chevalier C, Thiberge JM, Ferrero RL, Labigne A (1999) Essential role of*Helicobacter pylori* γ-glutamyltranspeptidase for the colonization of the gastric mucosa of mice. Mol. Microbiol. 31, 1359–1372.

[9] Gong M, Ho B (2004) Prominent role of γ-glutamyltranspeptidase on the growth of *Helicobacter pylori*. World J. Gastroenterol. 20, 2994–2996.

[10] Shibayama K, Kamachi K, Nagata N, Yagi T, Nada T, Doi Y et al. (2003) A novel apoptosis-inducing protein from *Helicobacter pylori*. Mol. Microbiol. 47, 443–451.

[11] Busiello I, Acquaviva R, Di Popolo A, Blanchard TG, Ricci V, Romano M et al. (2004) *Helicobacter pylori* γ-glutamyltranspeptidase upregulates COX-2 and EGF-related peptide expression in human gastric cells. Cell Microbiol. 6, 255–267.

[12] Barnes HA, Bagnall MC, Browning DD, Thompson SA, Manning G, Newell DG (2007) γ-Glutamyltranspeptidase has a role in the persistent colonization of the avian gut by *Campylobacter jejuni*. Microb. Pathog. 43, 198–207.

[13] Takahashi H, Hirose K, Watanabe H (2004) Necessity of meningococcalγ-glutamyl aminopeptidase for *Neisseria meningitidis* growth in rat cerebrospinal fluid (CSF) and CSF-like medium. J. Bacteriol. 186, 244–247.

[14] Lin LL, Chou PR, Hua YW, Hsu WH (2006) Overexpression, one-step purification, and biochemical characterization of a recombinant γ-glutamyltranspeptidase from *Bacillus licheniformis*. Appl. Microbiol. Biotechnol. 73, 103–112.

[15] Murty NAR, Tiwary E, Sharma R, Nair N, Gupta R (2012) γ-Glutamyltranspeptidase from *Bacillus pumilus* KS12: decoupling autoprocessing from catalysis and molecular characterization of N-terminal region. Enzyme Microb. Technol. 50, 159–164.

[16] Nakayama R, Kumagai H, Tochikura T (1984) Purification and properties of γ-glutamyltranspeptidase from *Proteus mirabilis*. J. Bacteriol. 160, 341–346.

[17] Ogawa Y, Hosoyama H, Hamano M, Motai H (1991) Purification and properties of γ-glutamyltranspeptidase from *Bacillus subtilis* (natto). Agric. Biol. Chem. 55, 2971–2977.

[18] Shuai Y, Zhang T, Mu W, Jiang B (2011) Purification and characterization of γ-glutamyltranspeptidase from *Bacillus subtilis* SK11.004. J. Agric. Food Chem. 59, 6233–6238.

[19] Suzuki H, Kumagai H, Tochikura T (1986) γ-Glutamyltranspeptidase from *Escherichia coli* K-12: purification and properties. J. Bacteriol. 168, 1325–1331.

[20] Lancaster JE, Shaw ML (1994) Characterization of purified γ-glutamyltranspeptidase in onions: evidence for in vivo role as peptidase. Phytochemistry. 36, 1351–1358.

[21] Martin MN, Slovin JP (2000) Purified γ-glutamyltranspeptidases from tomato exhibit high affinity for glutathione and glutathione S-conjugates. Plant Physiol. 122, 1417–1426.

[22] Castellano, I. and Merlino, A. (2012) γ-Glutamyltranspeptidases: sequence, structure, biochemical properties, and biotechnological applications. Cell Mol. Life Sci. doi: 10.1007s00018-012-0988-3.

[23] Okada T, Suzuki H, Wada K, Kumagai H, Fukuyama K (2006) Crystal structures of γ-glutamyltranspeptidase from *Escherichia coli*, a key enzyme in glutathione metabolism, and its reaction intermediate. Proc. Natl. Acad. Sci. USA. 103, 6471–6476.

[24] Suzuki H, Kumagai H (2002) Autocatalytic processing of γ-glutamyltranspeptidase. J. Biol. Chem. 277, 43536–43543.

[25] Boanca G, Sand A, Barycki JJ (2006) Uncoupling the enzymatic and autoprocessing activities of *Helicobacter pylori* γ-glutamyltranspeptidase. J. Biol. Chem. 281, 19029–19037.

[26] Lyu RC, Hu HY, Kuo LY, Lo HF, Ong PL, Chang HP et al. (2009) Role of the conserved Thr399 and Thr417 residues of *Bacillus licheniformis* γ-glutamyltranspeptidase as evaluated by site-directed mutagenesis. Curr. Microbiol. 59, 101–106.

[27] Chang HP, Liang WC, Lyu RC, Chi MC, Wang TZ, KL K.L. et al. (2010) Effects of C-terminal truncation on autocatalytic processing of *Bacillus licheniformis* γ-glutamyltranspeptidase. Biochemistry (Mos.). 75, 919–929.

[28] Castellano I, Merlino A, Rossi M, La Cara F (2010) Biochemical and structural properties of γ-glutamyltranspeptidase from *Geobacillus thermodenitrificans*: an enzyme specialized in hydrolase activity. Biochimie. 92, 464–474.

[29] Lobley A, Whitmore L, Wallace BA (2002) DICHROWEB: an interactive website for the analysis of protein secondary structure from circular dichroism spectra. Bioinformatics. 18, 211–212.

[30] Mao D, Wachter E, Wallace BA (1982) Folding of the mitochondrial proton adenosine triphosphatase proteolipid channel in phospholipid vesicles. Biochemistry. 21, 4960–4968.

[31] Royer CA (2006) Probing protein folding and conformational transitions with fluorescence. Chem. Rev. 106, 1769–1784.

[32] Ptitsyn OB (1995) Molten globule and protein folding. Adv. Protein Chem. 47, 83–229.

[33] Oinonen C, Rouvinen J (2000) Structural comparison of Ntn hydrolases. Protein Sci. 9(12), 2329–2337.

[34] Boanca G, Sand A, Okada T, Suzuki H, Kumagai H, Fukuyama K et al. (2007) Autoprocessing of*Helicobacter pylori* γ-glutamyltranspeptidase leads to the formation of a threonine–threonine catalytic dyad. J. Biol. Chem. 282(1), 534–541.

[35] Okada T, Suzuki H, Wada K, Kumagai H, Fukuyama K (2007) Crystal structure of the γ-glutamyltranspeptidase precursor protein from *Escherichia coli*: structural changes upon autocatalytic processing and implications for the maturation mechanism. J. Biol. Chem. 282(4), 2433–2439.

[36] Xu Q, Buckley D, Guan C, Guo HC (1999) Structural insights into the mechanism of intramolecular proteolysis. Cell. 98, 651–661.

[37] Ditzel L, Huber R, Mann K, Heinemeyer W, Wolf DH, Groll M (1998) Conformational constraints for protein self-cleavage in the proteasome. J. Mol. Biol. 279, 1187–1191.

[38] Kim JK, Yang IS, Rhee S, Dauter Z, Lee YS, Park SS et al. (2003) Crystal Structures ofglutaryl 7-aminocephalosporanic acid acylase: insight into autoproteolytic activation. Biochemistry. 42, 4084–4093.

[39] Choi KS, Kim JA, Kang HS (1992) Effects of site-directed mutations on processing and activities of penicillin G acylase from *Escherichia coli* ATCC 11105. J. Bacteriol. 174, 6270–6276.

[40] Lee YS, Park SS (1998) Two-step autocatalytic processing of theglutaryl 7-aminocephalosporanic acid acylase from *Pseudomonas* sp. strain GK16. J. Bacteriol. 180, 4576–4582.

[41] Kasche V, Lummer K, Nurk A, Piotraschke E, Rieks A, Stoeva S et al. (1999) Intramolecular autoproteolysis initiates the maturation of penicillin amidase from *Escherichia coli*. Biochim. Biophys. Acta. 1433, 76–86.

[42] Saarela J, Laine M, Tikkanen R, Oinonen C, Jalanko A, Rouvinen J et al. (1998) Activation and oligomerization of aspartylglucosaminidase. J. Biol. Chem. 273, 25320–25328.

[43] Schmidtke G, Kraft R, Kostka S, Henklein P, Frömmel C, Löwe J et al. (1996) Analysis of mammalian 20 S proteasome biogenesis: the maturation of β-subunits is an ordered two-step mechanism involving autocatalysis. EMBO J. 15, 6887–6898.

[44] Wang Y, Guo HC (2003) Two-step dimerization for autoproteolysis to activate glycosylasparaginase. J. Biol. Chem. 278, 3210–3219.

[45] Hung CP, ang JC, Chen JH, Chi MC, Lin LL (2011) Unfolding analysis of the mature and unprocessed forms of *Bacillus licheniformis* γ-glutamyltranspeptidase. J. Biol. Phys. 37, 463–475.

[46] Yang JC, Liang WC, Chen YY, Chi MC, Lo HF, Chen HL et al. (2011) Biophysical characterization of *Bacillus licheniformis* and *Escherichia coli* γ-glutamyltranspeptidases: a comparative analysis. Int. J. Biol. Macromol. 48, 414–422.

[47] Laemmli UK (1970) Cleavage of structural proteins during the assembly of the head of bacteriophage T4. Nature. 227, 680–685.

[48] Greenfield NJ (2004) Analysis of circular dichroism data. Meth. Enzymol. 383, 282–317.

[49] Royer CA, Mann CJ, Matthews CR (1995) Resolution of the fluorescence equilibrium unfolding profile of trp aporepressor using single tryptophan mutants. Protein Sci. 2, 1844–1852.

[50] Scholtz JM, Grimsley GR, Pace CN (2009) Solvent denaturation of proteins and interoretations of the *m* value. Meth. Enzymol. 466, 549–565.

[51] Nimlos MR, Matthews JF, Crowley MF, Walker RC, Chukkapalli G, Brady JW et al. (2007) Molecular modeling suggests induced fit of Family I carbohydrate-binding modules with a broken-chain cellulose surface. Protein Eng. Des. Sel. 20, 179–187.

[52] Arnold K, Bordoli L, Kopp J, Schwede T (2006) The SWISS-MODEL workspace: a web-based environment for protein structure homology modeling. Bioinformatics. 22, 195–201.